



HAL
open science

Crystallographic structure of vanadium carbide precipitates in a model Fe-C-V steel

Thierry Epicier, Daniel Acevedo-Reyes, Michel Perez

► **To cite this version:**

Thierry Epicier, Daniel Acevedo-Reyes, Michel Perez. Crystallographic structure of vanadium carbide precipitates in a model Fe-C-V steel. *Philosophical Magazine*, 2008, 88 (1), pp.31-45. 10.1080/14786430701753816 . hal-00513843

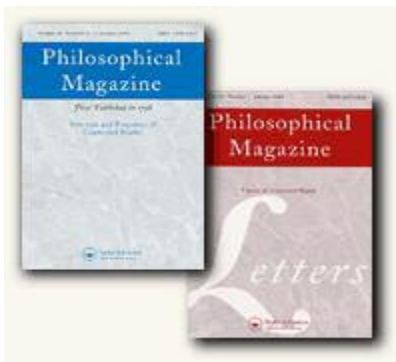
HAL Id: hal-00513843

<https://hal.science/hal-00513843>

Submitted on 1 Sep 2010

HAL is a multi-disciplinary open access archive for the deposit and dissemination of scientific research documents, whether they are published or not. The documents may come from teaching and research institutions in France or abroad, or from public or private research centers.

L'archive ouverte pluridisciplinaire **HAL**, est destinée au dépôt et à la diffusion de documents scientifiques de niveau recherche, publiés ou non, émanant des établissements d'enseignement et de recherche français ou étrangers, des laboratoires publics ou privés.



Crystallographic structure of vanadium carbide precipitates in a model Fe-C-V steel

Journal:	<i>Philosophical Magazine & Philosophical Magazine Letters</i>
Manuscript ID:	TPHM-07-Aug-0216.R1
Journal Selection:	Philosophical Magazine
Date Submitted by the Author:	31-Aug-2007
Complete List of Authors:	Epicier, Thierry; Université de Lyon, MATEIS Acevedo-Reyes, Daniel; ASCOMETAL, CREAS PEREZ, Michel; Université de Lyon, MATEIS
Keywords:	carbides, crystal structure, diffraction, high-resolution imaging, HRTEM, image simulation, precipitation, transmission electron microscopy
Keywords (user supplied):	carbides, crystal structure, diffraction
<p>Note: The following files were submitted by the author for peer review, but cannot be converted to PDF. You must view these files (e.g. movies) online.</p> <p>Epicier-PM-Resub.tex</p>	



Crystallographic structure of vanadium carbide precipitates in a model Fe-C-V steel

T. EPICIER*†, D. ACEVEDO†‡ and M. PEREZ †

†Université de Lyon - INSA de Lyon, MATEIS, UMR CNRS 5510, F-69621 Villeurbanne Cedex

‡ ASCOMETAL CREAS - Metallurgy, BP 70045, F-57301 Hagondange cedex

(v2.0 released July 2007)

The crystallographic structure of vanadium carbide precipitates in iron is investigated using High Resolution Transmission Electron Microscopy (HRTEM) and conventional Selected Area Diffraction (SAD) analysis. After a two steps precipitation treatment (10 hours at 700°C and 10 days at 800°C) and different annealing treatments (from 870°C to 920°C) performed on an ultra-pure Fe-V-C model alloy, carbides exhibit unambiguously the ordered monoclinic form V_6C_5 . The often reported V_4C_3 structure, that refers to the pioneer work by Baker and Nutting [R. G. Baker and J. Nutting, *Precipitation processes in steels* (1959)] is not encountered in the present investigation. Reasons for this contradiction will be discussed, and the conclusion is drawn that no literature data is available to unambiguously support the existence of precipitates with the V_4C_3 structure.

1 Introduction

Microalloyed steels have received considerable interest over many years because of their extensive use for many industrial applications [1]. As an example, addition of Vanadium and/or Niobium is a well-known way to control the mechanical properties of the alloy: (i) in Interstitial Free (IF) steels, carbonitride precipitation traps C and N atoms out of the solid solution, thus improving the formability [2]; (ii) in High-Strength Low-Alloyed (HSLA) steels, the grain size is controlled by a fine dispersion of carbonitride precipitates [1]. In this context, understanding the evolution of the precipitation state during the elaboration process of steels is a key to optimise its final properties. From an experimental point of view, it is then required to proceed to a detailed microstructural characterisation of the size, volume fraction, chemistry and crystallography of the precipitates. Such data are required for any attempt to model the kinetic evolution of the precipitation state versus temperature and time, as it is more and more achieved in modern thermodynamic approaches [3–6]. In the case of the well-documented Fe-V-C system, conflicting results can be found in the literature concerning the crystallography of vanadium carbide precipitates in ferrite: indeed, the B1, Na-Cl type stoichiometric VC or substoichiometric VC_{1-x} f.c.c. structure, the ordered V_6C_5 and V_4C_3 phases have been frequently reported (see below). It is the purpose of this paper to clarify the structure of the vanadium carbide precipitates encountered in the course of a thorough experimental and thermodynamic investigation of model Fe-V-C alloys [7,8].

2 Electron Microscopy work

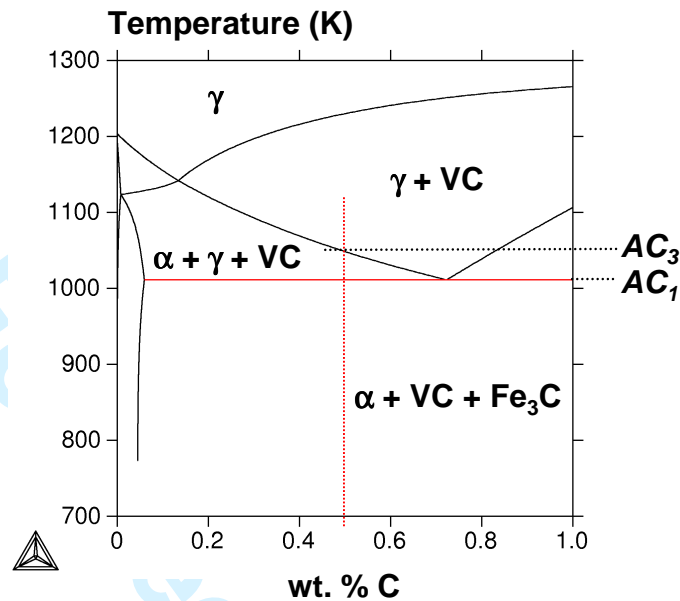
TEM observations of precipitates were performed on both thin foils and carbon extraction replicas. Thin foils serve to observe the location and orientation relationship, with respect to the matrix, of the precipitates, whereas extraction replicas allow easier statistics about the size of the precipitates¹. Thin foils were obtained by the conventional method of careful grinding to produce a thin disc of less than 50 μm (in order to minimise the undesirable magnetic effects in the TEM), followed by final thinning to electron transparency by ion beam thinning with argon ions at 4 to 2.5 keV under grazing incidence of 6 to 3° in

*Corresponding author. Email: thierry.epicier@insa-lyon.fr

¹According to a previous work on a similar steel, carbides as small as 3 nm are successfully extracted [9].

Table 1. composition of the laboratory Fe-V-C model steel (in wt.%)

C	V	S	O	N
0.48	0.20	< 0.0005	< 0.0005	< 0.0005

Figure 1. section of the Fe-V-C phase diagram at 0.2 wt. % V (Thermocalc calculation with PTER public database - <http://www.thermocalc.com>).

a Gatan PIPS instrument. Extraction replicas were obtained by a classical carbon film deposition (of an estimated thickness 15 - 30 nm) on the surface of samples polished to $\frac{1}{4}$ μm finish with diamond paste and slightly etched with a 0.4 % Nital solution. The final dissolution of the matrix is performed in an ethanol - nitric acid bath.

Electron microscopy was essentially performed using a JEOL 2010F field emission gun transmission electron microscope operating at 200 kV and equipped with an Oxford EDX device. The microscope was fitted with a JEOL annular detector allowing High Angle Annular Dark Field (HAADF) imaging in the scanning mode (STEM).

3 Alloy and Treatments

An ultra-pure model alloy, the composition of which is given in Table 1, has been specifically prepared by direct melting at 1450°C in an induction furnace under a mixed Ar/H₂ atmosphere (PECM laboratory of the Ecole des Mines de Saint-Etienne — lecoze@emse.fr).

A solutionizing treatment (30 minutes at 1000°C) followed by a water quench has been performed. A dedicated treatment to achieve a 'fully-precipitated state' has been designed according to the following considerations:

- (i) to ensure homogeneous nucleation, it was preferred to perform nucleation and growth stages in ferrite α -Fe; according to the Fe-V-C phase diagram (see figure 1), a treatment of 10 hours at 700°C in vacuum (quartz encapsulation), followed by a slow air cooling, has been chosen.
- (ii) in order to investigate a wide range of sizes, it is necessary to perform either long-term treatments, or high temperature heat treatments.
- (iii) in order to maximise the precipitated volume fraction, it is necessary to perform low temperature treatments.

From all preceding points, it is tempting to perform long-term treatments at 700°C. Figure 2 shows

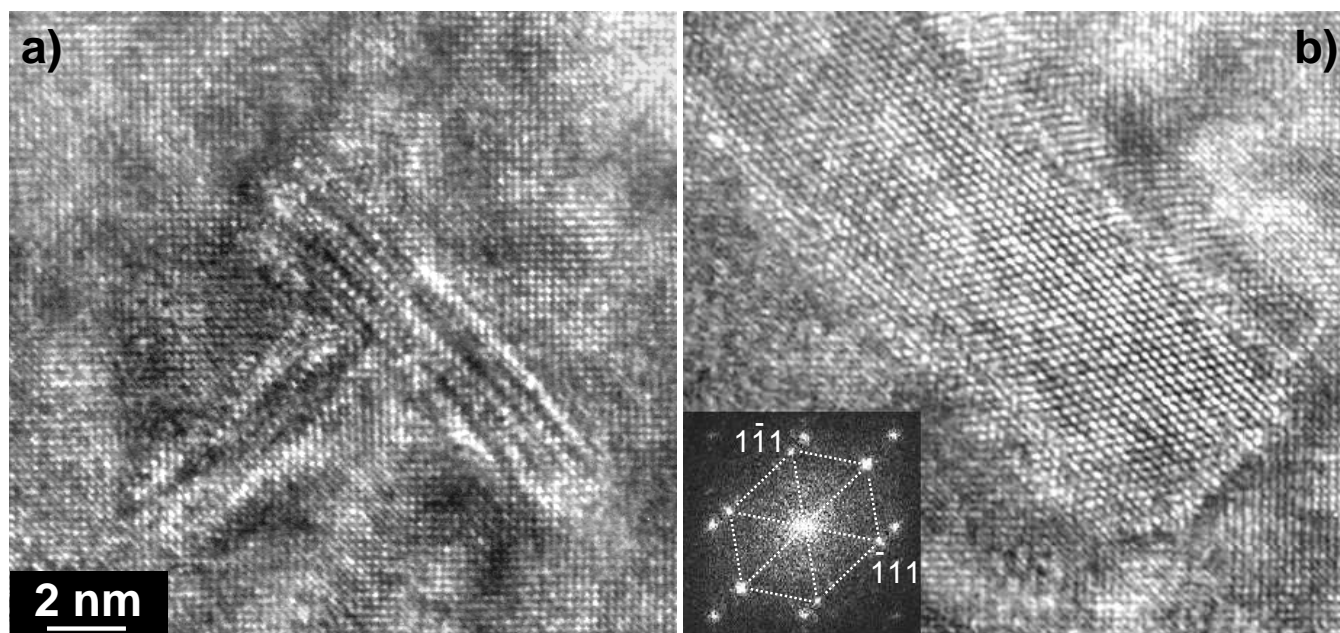


Figure 2. HRTEM imaging of Vanadium carbide precipitates within thin foils in a $[001]_{\text{Fe}}$ orientation after 10 hours at 700°C . The diffractogram on the right confirms the Baker-Nutting orientation relationship (the $[110]_{\text{fcc}}$ lattice section is underlined)

that the typical precipitate size after the initial nucleation treatment remains very small, of the order of a few nanometers. It also confirms that VC carbides adopt a fcc structure in the expected Baker-Nutting orientation relationship [10]:

$$\begin{aligned} [100]_{\text{Fe}} // [110]_{\text{VC}} \\ (002)_{\text{Fe}} // (002)_{\text{VC}} \end{aligned} \quad (1)$$

Trying to perform coarsening at 700°C would lead to unfeasible treatment times (see below). Thus, an additional coarsening treatment of 10 days at 800°C (followed by a slow air cooling¹) has been decided. Choosing lower temperatures, as suggested by consideration (iii) above, would lead us to penetrate the rather complex 3-phases domain ($\alpha\text{-Fe} + \gamma\text{-Fe} + \text{carbide}$) between AC_1 and AC_3 temperatures (see figure 1), which is not desired. Figure 3 shows the resulting microstructure, and figure 3(a) demonstrates a distribution of roughly spherical precipitates, in the range 15-60 nm, within a ferritic grain. In order to get comparable precipitate sizes at 700°C , heat treatments as long as 100 days would have been necessary².

As a conclusion, 10 hours at 700°C followed by 10 days at 800°C and slow air cooling (designated as the “fully-precipitated state”³ herebelow) represents the best compromise to satisfy the three preceding points (i) to (iii). In order to further investigate a wide range of sizes, the alloy was subjected to different isothermal reversion treatments in the austenitic domain at 870°C (2 minutes and 60 minutes in a molten salt bath) and 920°C (60 minutes in a molten salt bath and 10 days in quartz capsules), followed by a water quench.

¹The iron austenitic matrix at 800°C turns into a ferrite-perlitic microstructure after the slow air cooling.

²According to the basic assumptions that (i) the coarsening is limited by Vanadium diffusion, and (ii) a characteristic diffusion distance ranges as \sqrt{Dt} , where D is the diffusion coefficient at a given temperature T ($D = 0.6110^{-4} \exp[-267100/RT]$ for V in ferrite, and $D = 0.2510^{-4} \exp[-264200/RT]$ for V in austenite $\gamma\text{-Fe}$ [1], with R equal to 8.32 J/K), 100 days at 700°C is “equivalent” to 10 days at 800°C .

³According to electrolytic dissolution and plasma spectroscopy, 80% of the vanadium is precipitated in that state [8].

4 Results

The crystal structure of vanadium carbide precipitates has been studied for each heat treatment (see section 3) on both thin foils and extraction replicas.

As already presented, Figure 3 is a montage from the 'fully-precipitated state'. All the precipitates that have been observed in thin foils appear to have a similar rounded-shape and were identified as fully incoherent with the matrix, owing to the absence of any orientation relationship¹ as revealed in diffraction mode. It was thus quite difficult to get crystallographic information on the precipitates in diffraction, since tilting experiments in magnetic materials is a very delicate task. However, in the case of figure 3, it has been possible to observe both matrix and precipitate reflections in a single diffraction pattern for one particle (b). The faint, vertically aligned spots arising from the precipitate are the unambiguous signature of the ordered V_6C_5 phase as explained by figure 3-c to f). In (c) and (d), well-oriented diffraction patterns, respectively obtained on a $VC_{\approx 0.84}$ single crystal [13], and on a Nb_6C_5 powder [14] are reported to serve as 'references' for the monoclinic B2/m [11] and hexagonal P3₁ [12] M_6C_5 superstructures (M=V or Nb), depicted in (e) and (f) respectively².

From a simple comparison between the experimental diffraction (b) and the 'standard' ones in (c) and (d), the monoclinic M_6C_5 ordered form is unambiguously identified for the precipitate of interest.

Figure 4 is a montage of conventional TEM and HAADF images after different thermal treatments, which further confirm the V_6C_5 monoclinic ordered form (*e.g.* figure 4(g)). The diffraction patterns in figure 4(e-f) show two variants of the V_6C_5 superstructure observed along equivalent $\langle 110 \rangle_{fcc}$ directions, but in this case the monoclinic form cannot be unambiguously identified since the hexagonal V_6C_5 cell exhibits reciprocal lattice sections with the same symmetry for both patterns (see Appendix).

During our extensive TEM observations, the positive identification of a M_6C_5 ordering (either the *M* or *H* phases, and preferably the *M* phase) has been systematic for all precipitates that could have been oriented along an adequate direction, in which superlattice reflections are expected. However, an undesirable irradiation effect was observed, as demonstrated in figure 5. Owing to knock-on damage arising from the incident primary electrons, disordering of the carbon-vacancy distribution occurred in a few seconds with the intense beam of the FEG-TEM. This phenomenon is well-known in the V_6C_5 [15] and V_8C_7 [16] ordered superstructures.

5 Discussion

From the above, the crystal structure of vanadium carbide precipitates has been positively identified as the M_6C_5 ordered phase, and most probably the monoclinic form proposed by [11].

Nevertheless, some ambiguity remains concerning the precipitates observed in $\langle 110 \rangle_{fcc}$ orientations, directly after the nucleation treatment of 10 hours at 700°C (see figure 2). Indeed, it has been shown in figure 5(b) that unirradiated ordered V_6C_5 particles exhibit a doubling of the $(111)_{fcc}$ lattice fringes in $\langle 110 \rangle_{fcc}$ HRTEM images. This feature is not observed in figure 2, which could suggest that the corresponding precipitates are not ordered and consequently with a composition possibly different from V_6C_5 . However, this conclusion cannot be ascertained for the following reasons:

- (i) in the monoclinic M_6C_5 form, some $\langle 110 \rangle_{fcc}$ -type zone axes do not exhibit any superlattice reflection (as discussed in the Appendix), which obviously prevents from seeing any doubling of $(111)_{fcc}$ lattice fringes;
- (ii) for those precipitates lying in rather thick matrix region (figure 2(a)), the existence of Moiré fringes makes it difficult to visualise the possible doubling of the $(111)_{fcc}$ lattice fringes;
- (iii) for those precipitates lying in rather thin region, without any significant overlapping matrix (figure 2(b)), the low thickness can prevent from seeing any fringe doubling. Although the quality of the

¹The initial Baker-Nutting [10] orientation relationship between precipitates and the ferritic matrix at 700°C (see Figure 2) has been lost during the subsequent coarsening treatment at 800°C in the austenitic domain.

²More details on the M_6C_5 ordered phases is given in Appendix.

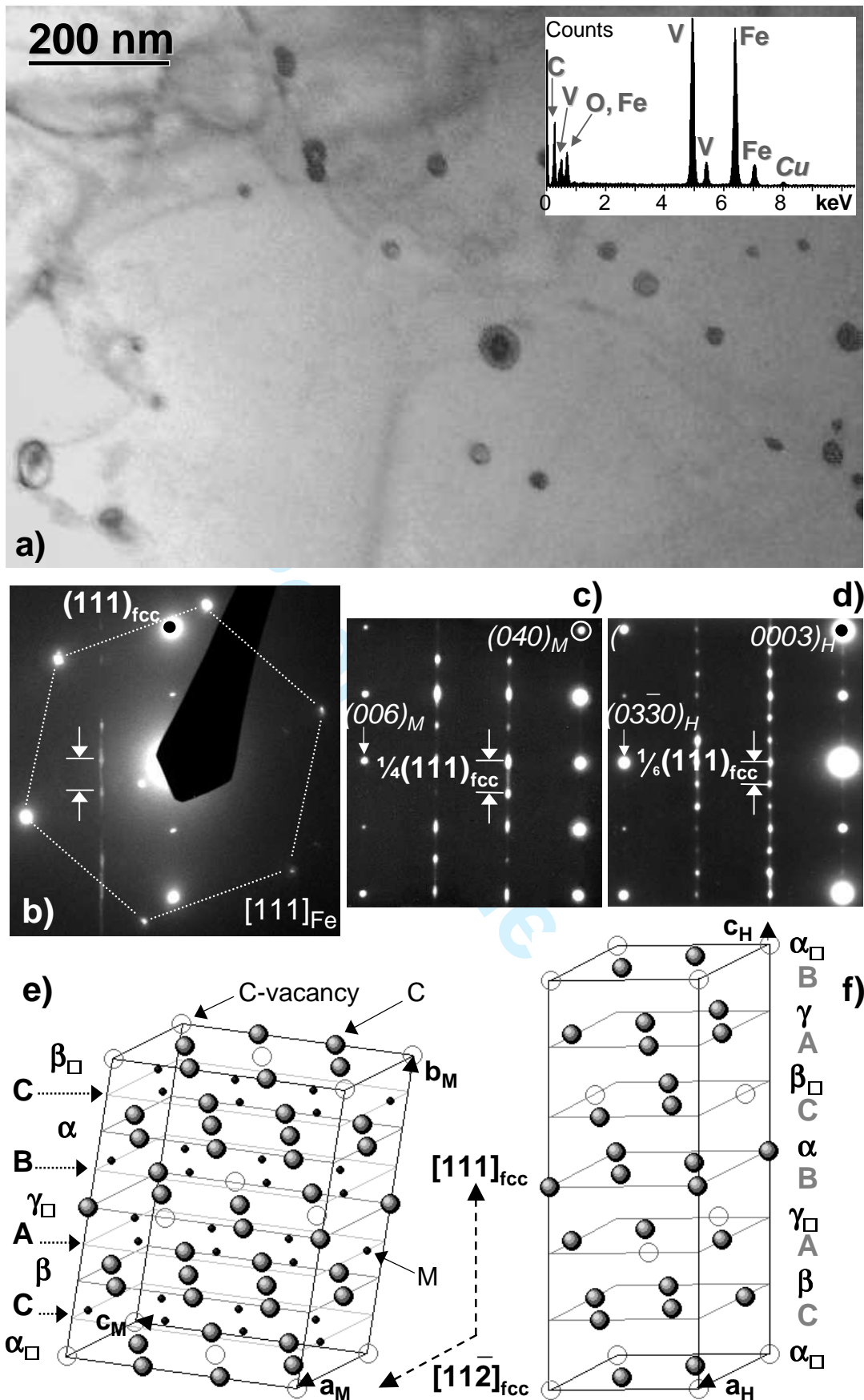


Figure 3. Precipitation structure in the as-received state. (a): Low magnification image showing 'spherical' precipitates in a grain of ferrite. Inset is a typical EDX spectrum acquired with a nano-probe on a single particle. (b): Diffraction pattern showing the α -Fe matrix near the $[111]_{fcc}$ orientation (dashed 'hexagon') and additional spots due to a precipitate (the $(111)_{fcc}$ reflection is labelled - see text for details). (c): $[100]_M$ diffraction pattern from a V_6C_5 'standard' ordered in the monoclinic (M) form [11], with $a_M = 0.509$, $b_M = 1.018$, $c_M = 0.882$ nm, $\gamma = 109.47^\circ$ (space group B2/m). (d): $[100]_H$ ($[2\bar{1}10]_H$ in four-indexes) diffraction pattern from a Nb_6C_5 'standard' ordered in the hexagonal (H) form [12], with $a_H = 0.546$, $c_H = 1.545$ nm (space group P31) - this pattern has been rescaled to be directly comparable to (c). (e): cell of the M_6C_5 monoclinic superstructure. Interstitial (111) carbon planes are labelled α , β and γ ; the symbol \square stands for planes containing vacancies. (f): *idem* (e) for the hexagonal superstructure (for clarity, M atoms have been omitted).

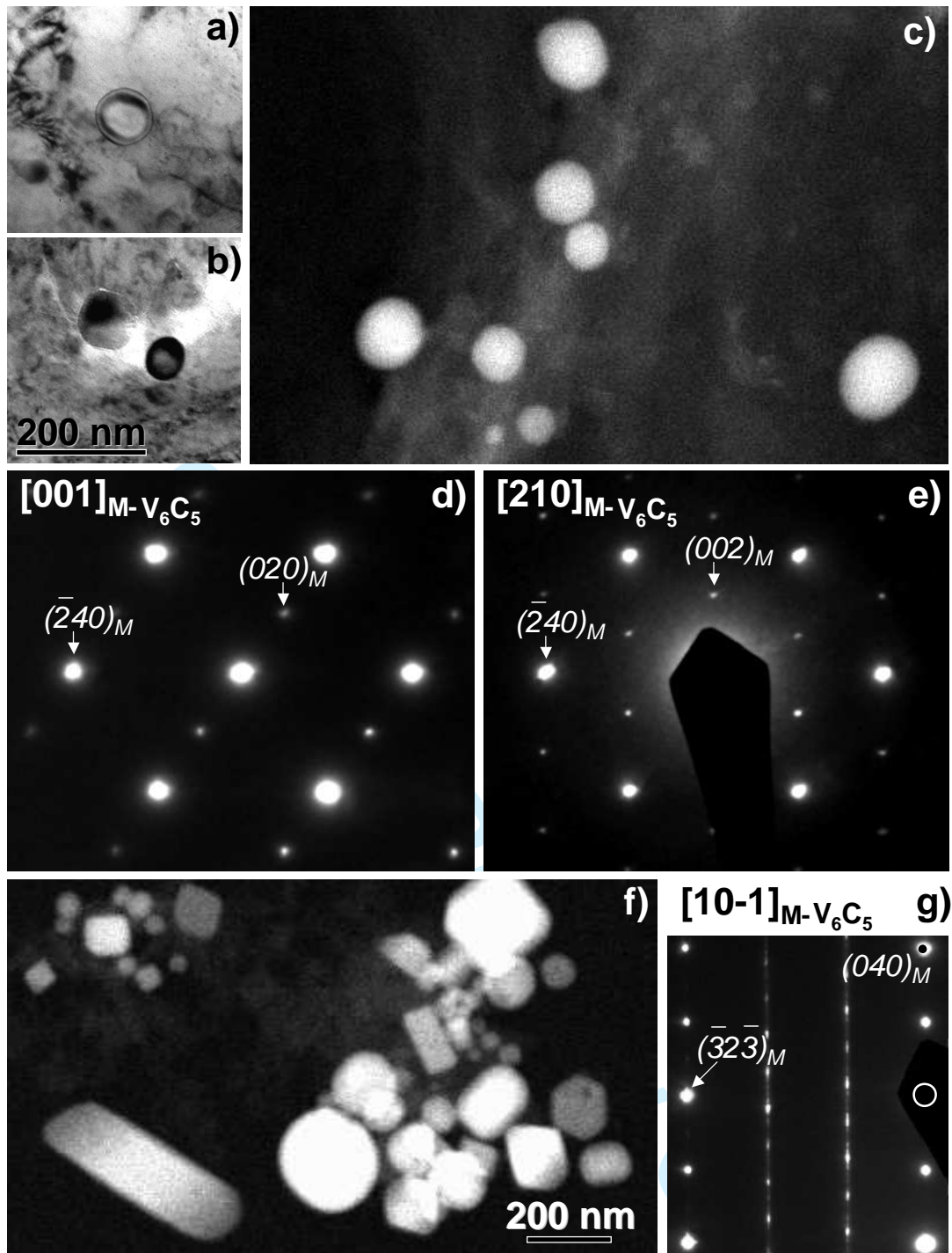


Figure 4. Evolution of precipitation during ageing. (a): Detail showing a precipitate in thin foil after 2 minutes at 870°C (TEM bright field). (b): *idem* (a) after 60 minutes at 920°C. (c): extraction replica of same state as in (b) observed in HAADF-STEM. (d-e): SAD patterns from two precipitates from (c) showing the unambiguous evidence of the V_6C_5 superstructure (the indexing is given for the monoclinic form, see text for details). (f): HAADF image of an extraction replica after 10 days at 920°C; larger and more cuboidal precipitates are observed. (g): further SAD evidence of the M- V_6C_5 ordered phase in state (f).

micrograph in figure 2(a) is not sufficient to allow HRTEM image simulation, indicative computations can be performed as a function of reasonable thicknesses and defoci for both ordered V_6C_5 and disordered VC (or VC_{1-x}). Figure 6 shows that for thin precipitates, the ordered phase can easily be misled with the disordered one for many defocus values, where the $\frac{1}{2}(111)_{fcc}$ superlattice fringes are too faint to be discerned.

(iv) As clearly evidenced by figure 5(d-f), electron irradiation promotes disordering, obviously all the more

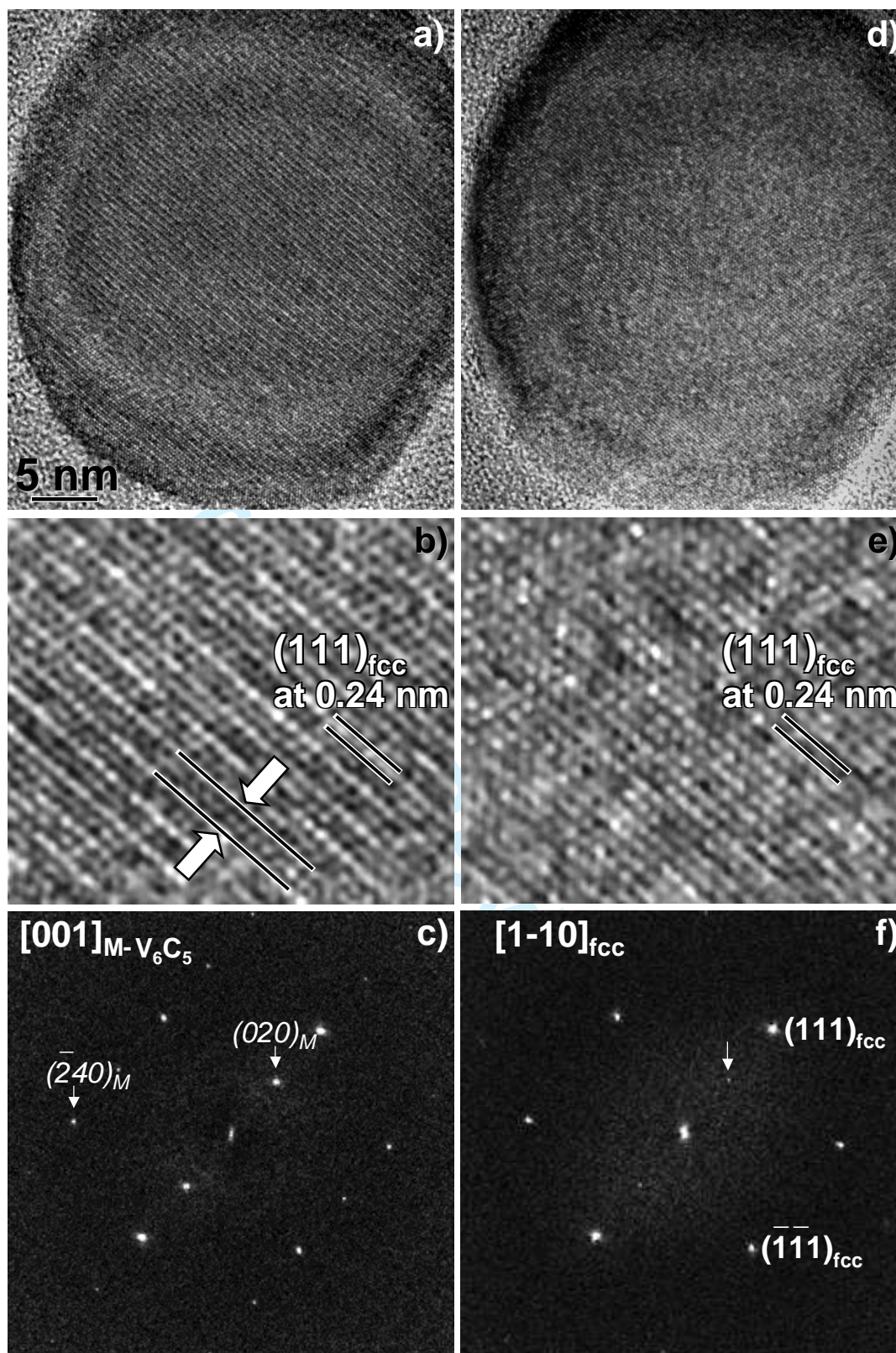


Figure 5. Irradiation damage of precipitates (after 60 minutes at 870°C). (a): $[1\bar{1}0]_{fcc}$ HRTEM image of a precipitate on an extraction replica. (b): Enlargement of the central part of the particle shown in (a): note the contrast re-enforcement every two $(111)_{fcc}$ lattice fringes (arrows), due to carbon ordering in the V_6C_5 structure. (c): numerical diffractogram from (b) showing the $\frac{1}{2}(111)_{fcc} = (020)_M$ superlattice reflection responsible for the fringes doubling in (b). (d-f): same as (a-c) after 30 seconds under the electron beam: note that the $(020)_M$ superlattice fringes and reflection have almost vanished in (e) and (f) respectively. Note that the HRTEM contrast of images (b) and (e) is not excellent because of the thick particle and the additional carbon replica layer.

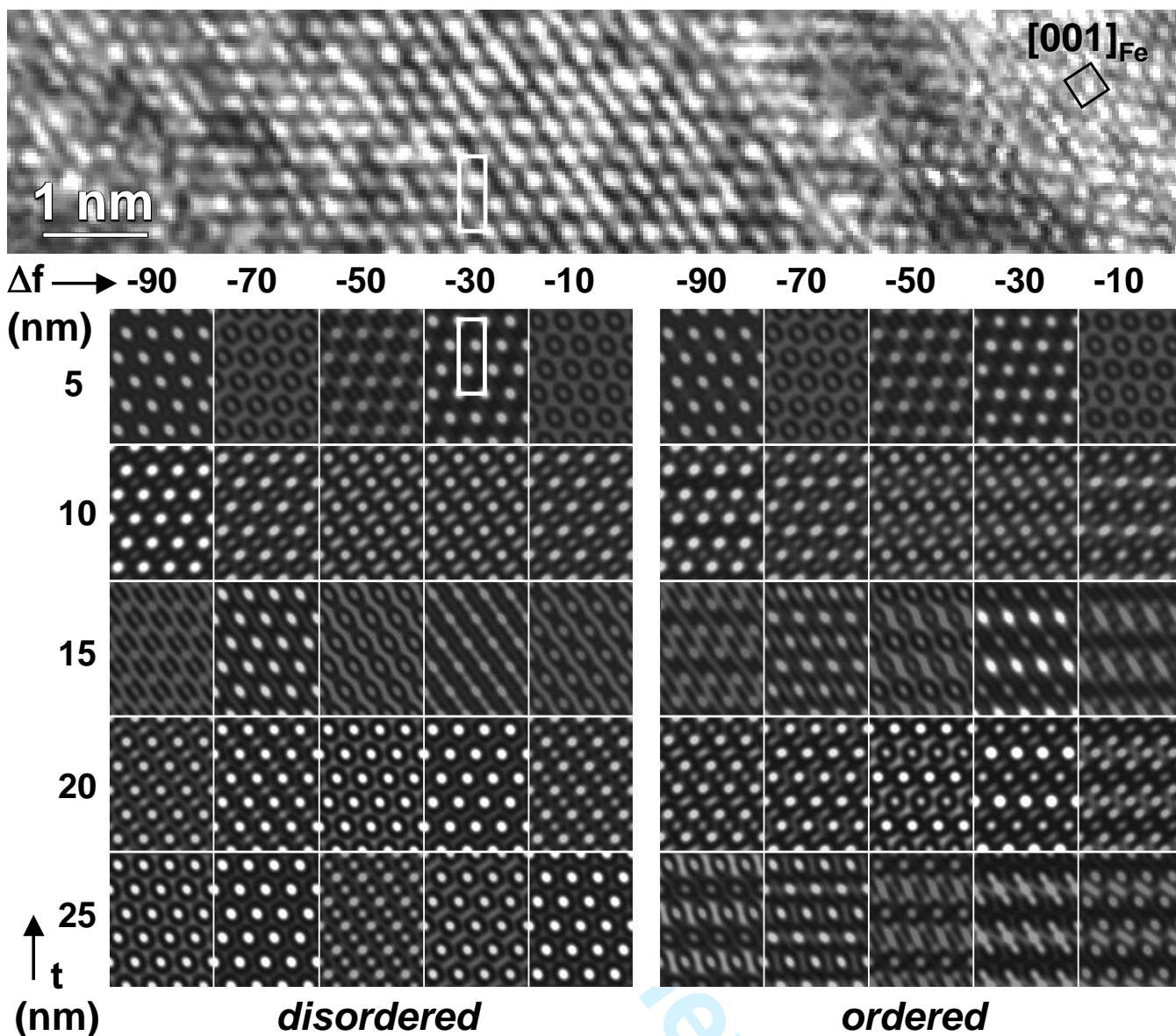


Figure 6. HRTEM simulations of both disordered and ordered forms of V_6C_5 structure. An enlarged detail of the experimental numeric micrograph b) from Figure 2 is reported on the top (after re-orientation consistently with the simulations, according to the superimposed white frame). Note that depending on the thickness and defocus combination (t and Δf , respectively plotted vertically and horizontally), both structures frequently lead to comparable features where ordering cannot be identified (simulations performed with typical imaging parameters for the JEOL2010F microscope with a home-made program, W-SIMPLY [17]).

easily than the crystal is thin.

In complement to High Resolution imaging, one may think of performing nano-diffraction. It should be emphasised that such observations remain rather difficult owing to (i) the size of the particles embedded in the matrix, and (ii) the high electron beam flux inherent to this mode, which would promote fast irradiation effects.

As a conclusion, the smallness of vanadium carbides present after 10 hours at 700°C prevents from any positive interpretation of the ordering state and consequently of the chemical composition. Note that in all other states where precipitates were large enough to allow a classical electron diffraction analysis, the ordered V_6C_5 phase was unambiguously identified.

Surprisingly, although works on the precipitation of vanadium carbide in steels report the existence of the V_6C_5 structure [18–20], or simply refer to the fcc, B1-type VC_{1-x} structure [21–24], a lot of them, moreover rather recent, claim evidence for the " V_4C_3 " structure [25–31] in most cases with the simple

1 indication of a fcc lattice parameter near or equal to 0.416 nm, as already mentioned in the pioneer works
2 on precipitation of metallic carbides in low-alloy steels (*e.g.* [32,33]). Even in the well-known work by Baker
3 and Nutting on (Mo,V)C precipitates in steel [10], V_4C_3 is mentioned all-through the paper. Moreover,
4 these authors pointed out the experimental evidence of unknown extra-spots in an electron diffraction
5 pattern: these extra-spots are indeed fully consistent with superlattice reflections due to the V_6C_5 phase,
6 unknown at this time!

7
8 In fact the composition M_4C_3 refers to the M_4C_3 or ζ - MC_{1-x} structure, as identified in the transi-
9 tion metal carbides of the Vth group (VC, NbC and TaC), at the phase boundary between the cubic
10 monocarbide MC_{1-x} and the hexagonal hemicarbide M_2C [34]. However, an obsolete 'deleted' JCPDS file
11 (# 01-1159) describes V_4C_3 as a simple fcc, B1-type structure (space group Fm3m) with $a = 0.416$ nm,
12 which can account for indexing errors (*i.e.* V_4C_3 instead of the Na-Cl monocarbide VC_{1-x} - see for exam-
13 ple [35]). It is worth noting that in a previous study on carbides in cast iron [19], the authors mention the
14 same statement, that is no evidence is reported in the literature of the $\zeta - MC_{1-x}$ phase in the carbides
15 labelled $VC_{0.75}$ or V_4C_3 in multi-components alloys.

16
17 According to the detailed crystallographic analysis of the M_4C_3 phase reported in the Appendix, it can
18 be concluded that: (i) the ordered V_6C_5 phase unambiguously identified here cannot be confused with the
19 V_4C_3 phase; (ii) since we are not aware of any positive identification of the V_4C_3 through an unambiguous
20 electron diffraction experiment in the previously mentioned literature, the hypothesis that V_4C_3 has been
21 invoked instead of the V_6C_5 phase, or simply a fcc VC_{1-x} phase, is indeed very probable.

22 Obviously, Electron Energy Loss Spectroscopy (EELS) would allow the chemical composition of pre-
23 cipitates to be ascertained (but not directly their crystallography). Such experiments require a delicate
24 calibration procedure, using normalised reference spectra for the Vanadium-L and Carbon-K edges, as was
25 recently done in the case of niobium carbonitrides [9]. Moreover, EELS analysis obviously requires to get
26 rid of any spurious carbon signal: this appears to be very delicate to achieve in the case of thin foils (due
27 to carbon contamination and poor signal to noise ratio) and, *a fortiori* in the case of carbon extraction
28 replicas [36]. Nevertheless, the basic crystallographic analysis in TEM remains an elegant way to evaluate
29 the chemical composition of sub-stoichiometric metal carbides, which is associated to different long- and
30 short-range ordered states (among them, the V_6C_5 and V_4C_3 forms), easily identified in diffraction and
31 HRTEM modes [14, 16].
32
33
34
35
36
37
38
39
40

41 6 Conclusions

- 42
43 (i) After a specific two-step heat treatment (10 hours at 700°C and 10 days at 800°C) designed to get
44 coarse vanadium precipitates, different reversion treatments (from 870°C to 920°C) led to precipitates
45 ranging from 10 to 200 nm in size. All analysed precipitates have been positively identified as monoclinic
46 ordered V_6C_5 carbides, and no evidence has been obtained for the V_4C_3 structure.
47 (ii) Due to knock-on damages arising from incident primary electrons, disordering of the carbon-vacancy
48 distribution within precipitates occurred in a few seconds with the intense beam of the FEG-TEM.
49 (iii) Precipitates resulting from the 10 hours at 700°C treatment were too thin to be unambiguously iden-
50 tified as monoclinic ordered V_6C_5 carbides.
51 (iv) Many authors report the presence of ordered V_4C_3 structure for vanadium carbide precipitates, often
52 referring to the famous paper by Backer and Nutting. However, the description of the diffraction
53 pattern made by Backer and Nutting corresponds surprisingly well with the monoclinic ordered V_6C_5
54 structure, that was unknown at this time.
55 (v) To our knowledge, no unambiguous diffraction experiment has been performed in the literature, which
56 positively identifies the V_4C_3 structure within precipitates. It seems thus that the often reported V_4C_3
57 precipitates structure could be V_6C_5 instead.
58
59
60

7 Acknowledgements

The authors are grateful to the CLYME (Consortium Lyonnais de Microscopie Electronique) for the access to the JEOL 2010F microscope. This work was financially supported by Ascometal and thanks are due to P. Dierickx (CREAS) for fruitful discussion.

Appendix A: additional comments on the M_6C_5 and M_4C_3 phases in the V-C system

A.1 The V_6C_5 ordered structure and crystallographic analysis of Figure 3.

Basically, the fcc-based, Na-Cl or B1-type structure of the transition metal carbides such as VC_{1-x} , NbC_{1-x} , accommodates the departure from stoichiometry (x) by the presence of constitutional vacancies within the carbon sublattice. Ordering at the M_6C_5 ($MC_{\approx 0.833}$) composition is due to the regular succession of full and vacancy-containing interstitial carbon close-packed planes in a given $[111]_{\text{fcc}}$ direction, with determines the longest repeat distance of the ordered phase. In the case of the monoclinic structure (M), the periodicity is established by the stacking of 4 such “basal” planes, and the complete sequence of both metal and carbon $(111)_{\text{fcc}}$ planes can be written as:

$$\alpha_{\square} C \beta A \gamma_{\square} B \alpha C \beta_{\square}$$

where greek and roman letters represent respectively the metalloid and metal layers, while the “ \square ” subscript indicates the vacancy-containing interstitial planes.

In this sequence, it clearly appears that the starting and ending (carbon+vacancy) planes are not of the same type (α_{\square} and β_{\square}), which explains why the b_M parameter defined by sequence is not along the $[111]_{\text{fcc}}$ direction, leading to a monoclinic cell (the angle γ between the \mathbf{b}_M axis and the \mathbf{a}_M axis lying in the $(111)_{\text{fcc}}$ ‘basal’ plane is 109.47°). The parameters of this monoclinic superlattice are ideally related to the parameter of the fcc disordered carbide ($a_{\text{fcc}} \approx 0.416$ nm for $VC_{0.833}$) through the analytical relations:

$$\mathbf{a}_M = \frac{1}{2}[11\bar{2}]_{\text{fcc}} \quad \left(a_M = \sqrt{\frac{3}{2}} a_{\text{fcc}} \right)$$

$$\mathbf{b}_M = [112]_{\text{fcc}} \quad \left(b_M = \sqrt{6} a_{\text{fcc}} \right)$$

$$\mathbf{c}_M = \frac{3}{2}[1\bar{1}0]_{\text{fcc}} \quad \left(c_M = \frac{3}{\sqrt{2}} a_{\text{fcc}} \right)$$

Similarly, the hexagonal superlattice (H) shown in figure 3(f) is based on a repeat sequence of 6 interstitial planes:

$$\alpha_{\square} C \beta A \gamma_{\square} B \alpha C \beta_{\square} A \gamma B \alpha_{\square}$$

In this case, the c_H axis defined by this sequence is parallel to the $[111]_{\text{fcc}}$ direction. As for the monoclinic structure, the parameters of this hexagonal superlattice are simply related to the parameter a_{fcc} ($a_{\text{fcc}} \approx 0.446$ nm for $NbC_{0.833}$):

$$\mathbf{a}_H = \frac{1}{2}[11\bar{2}]_{\text{fcc}} \quad \left(a_H = \sqrt{\frac{3}{2}}a_{\text{fcc}} \right)$$

$$\mathbf{c}_H = 2[111]_{\text{fcc}} \quad \left(c_H = 2\sqrt{3}a_{\text{fcc}} \right)$$

From these descriptions, it can easily be understood that the $\langle 112 \rangle_{\text{fcc}}$ azimuths are of special interest for identifying which ordered form occurs in V_6C_5 : one of this axis (*i.e.* $[11\bar{2}]_{\text{fcc}}$) is strictly the $[100]$ direction of both structures, with the 'basal' planes in zone. Then, in the case of the monoclinic phase, the reciprocal lattice vector $(111)_{\text{fcc}} = (040)_M$ is possibly divided into 4, as for the parallel rows (see figure 3(c)), while a division by 6 of the $(0006)_H = (111)_{\text{fcc}}$ vector is expected in the hexagonal structure (figure 3(d)).

The experimental pattern in figure 3(b) exhibits a division by 4, and does unambiguously correspond to the monoclinic form of V_6C_5 . This agrees well with a previous work on 'bulk' materials, which has shown that the monoclinic form is much more frequent than the hexagonal one in the case of vanadium carbide [14].

A.2 The V_4C_3 structure

The M_4C_3 structure was initially suggested in the region $VC_{0.50} - VC_{0.74}$ below 1344°C [37]. It was refined by X-Ray diffraction (JCPDS file # 35-0786 in the case of V_4C_3) in the V-C, Nb-C and Ta-C systems [34], and further confirmed by TEM in the V-C [38] and Ta-C [39, 40] systems.

According to the notations given in section A.1, the repeat sequence of the M_4C_3 structure can be written as a stacking of 12 metallic close-packed planes [34]:

$$A \gamma B \gamma A \gamma B \alpha C \beta A \beta C \beta A \gamma B \alpha C \alpha B \alpha C \beta A$$

Consequently, the structure appears to be of trigonal (T) symmetry (space group $R\bar{3}m$), with $a_T = 0.2917$ and $c_T = 2.783$ nm. In the original X-ray diffraction work by [34], the question of possible ordering of constitutional carbon vacancies could not be addressed. TEM work shows that short-range ordering exists in the case of V_4C_3 [38], whereas periodic removal of complete carbon layers is supposed in the case of Ta_4C_3 [39, 40]. However, the exact distribution of carbon atoms within the interstitial α , β and γ planes remains questionable; hence, the greek letters in the sequence written above designate carbon planes with averaged $\frac{3}{4}$ occupancies. But what is essential to note here is that this structure differs from the fcc-based MC_{1-x} structure, since the stacking of the close-packed metallic planes (*e.g.* A B A B C A C A B C B C) is a mixture of hcp and fcc layers. As for the M_6C_5 structures, the parameters of this trigonal superlattice are simply related to the parameter a_{fcc} :

$$\mathbf{a}_T = \frac{1}{2}[11\bar{2}]_{\text{fcc}} \quad \left(a_T = \sqrt{\frac{3}{2}}a_{\text{fcc}} \right)$$

$$\mathbf{c}_T = 4[111]_{\text{fcc}} \quad \left(c_T = 4\sqrt{3}a_{\text{fcc}} \right)$$

A.3 Comparing both V_4C_3 and V_6C_5 structures

At a first sight, V_4C_3 and V_6C_5 phases exhibit strong similarities in both imaging and diffraction modes: on the one hand, faulted microstructures are observed for both phases in bright or dark field micrographs

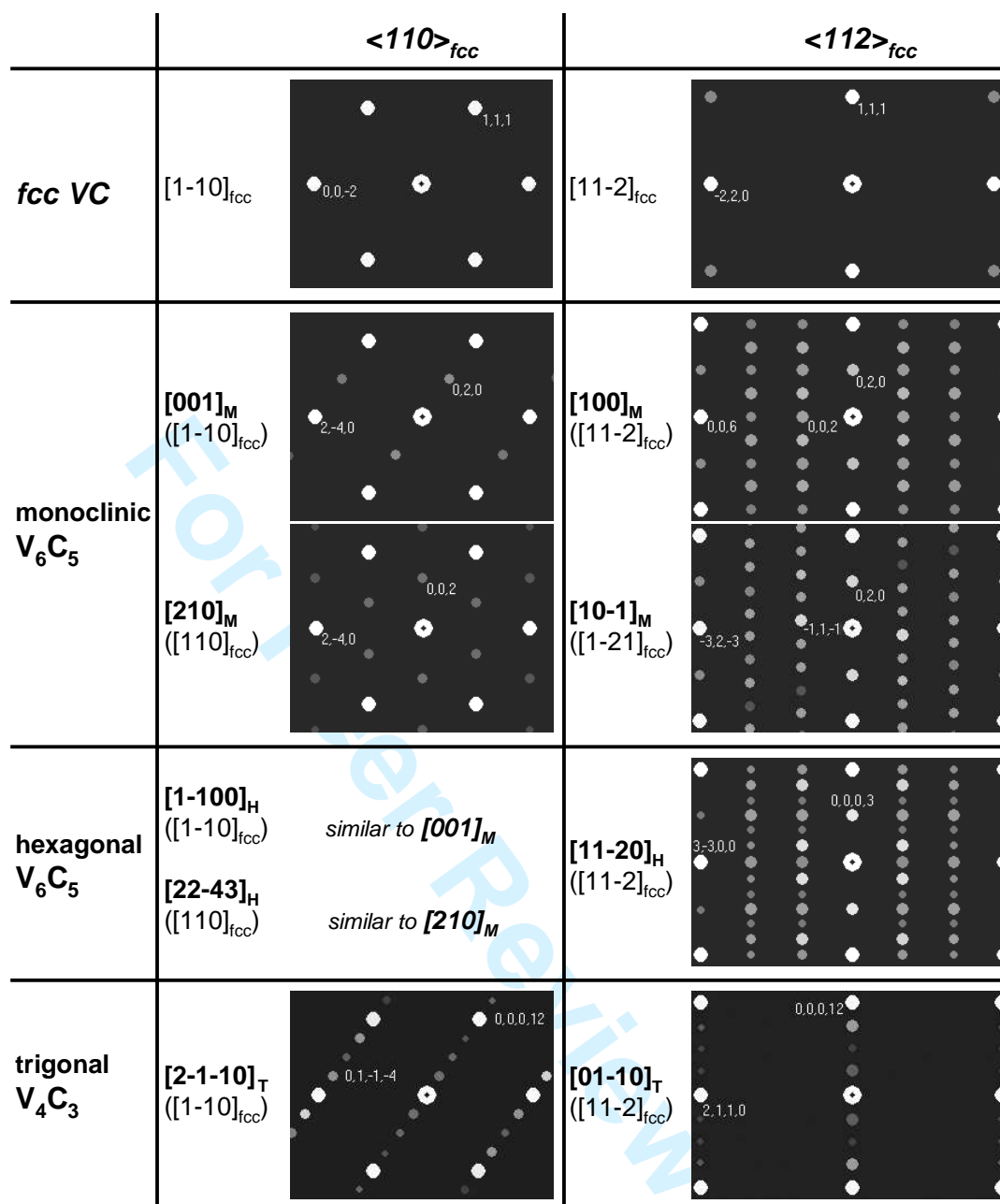


Figure A1. Montage showing kinematical diffraction patterns calculated for the fcc-VC, M- and H- V_6C_5 , and T- V_4C_3 structures in some low-index azimuths revealing their symmetries (see text for details; the spot patterns have been calculated with W-SIMPLY [17]).

(see [38–40]); on the other hand, faint 'superlattice-type' reflections occur in diffraction patterns, as shown in figure A1¹. However, these similarities are due to very different origins: in V_4C_3 , such features arise from stacking faults within the metallic sublattice, whereas they are caused by ordering of carbon-vacancies in V_6C_5 .

A detailed examination of the most significant diffraction patterns allows both structures to be discerned. Let us for example compare the $\langle 110 \rangle_{fcc}$ reciprocal lattice sections of both V_6C_5 and V_4C_3 structures in figure A1. In the T- V_4C_3 phase, superlattice reflections occur at $\frac{1}{4}(111)_{fcc}$, $\frac{1}{2}(111)_{fcc}$ and $\frac{3}{4}(111)_{fcc}$ (that

¹This montage summarises some of the $\langle 110 \rangle_{fcc}$ and $\langle 112 \rangle_{fcc}$ reciprocal lattice sections of the various forms of V_6C_5 , as indexed in the disordered cubic structure. For the sake of brevity, only most significant zone axes are shown. In the case of the monoclinic phase, it must be emphasised that the $[032]_M$ and $[0\bar{3}2]_M$ diffraction patterns (respectively $[101]_{fcc}$ and $[011]_{fcc}$) do not exhibit any superlattice reflections, which may correspond to what is observed in Figure 2 (as discussed in section 5).

is, $(0003)_T$, $(0006)_T$ and $(0009)_T$, while only one authorised additional spot occurs at $\frac{1}{2}(111)_{fcc}$ for the $M-V_6C_5$ form ($(020)_M$ in the $[001]_M$ zone axis), and equivalently for the $H-V_6C_5$ form (in the $[1\bar{1}00]_H$ zone axis). Moreover, kinematical calculations show that no multi-diffraction effect could make appear $\frac{1}{4}(111)_{fcc}$ -type diffraction spots in V_6C_5 . Regarding the $\langle 112 \rangle_{fcc}$ reciprocal lattice sections, the presence of diffractions rows at $\frac{1}{3}(\bar{2}20)_{fcc}$ and $\frac{2}{3}(\bar{2}20)_{fcc}$ proves unambiguously the existence of the V_6C_5 structure.

According to the above analysis, the present experimental results (e.g. Figure 4) lead to the following conclusions: (i) the V_6C_5 structure is positively identified in the $\langle 112 \rangle_{fcc}$ zone axes (furthermore in the monoclinic form - see main text for details -), (ii) the V_4C_3 structure is incompatible with the $\langle 110 \rangle_{fcc}$ diffraction patterns.

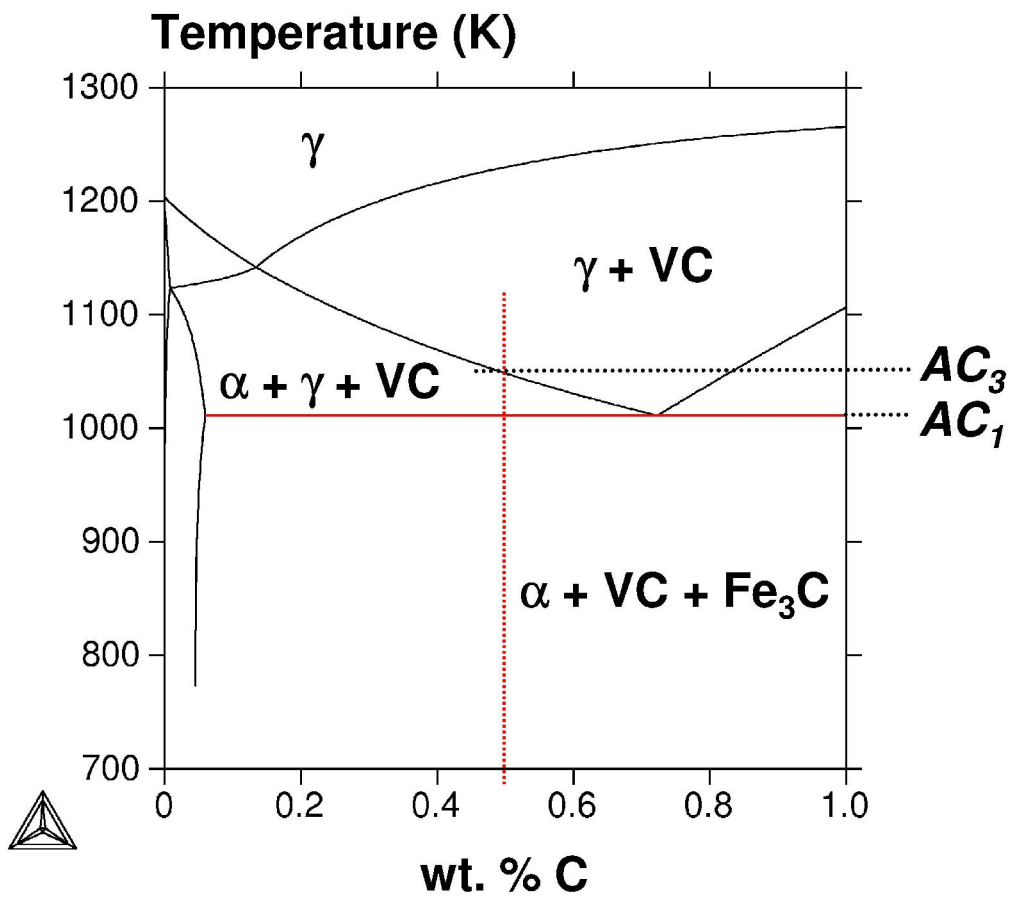
Surprisingly, none of these significant and unambiguous V_4C_3 diffraction patterns is reported in any of the numerous works that refer to the V_4C_3 phase in studies of vanadium carbide precipitation in ferrite (see references cited in the main text, section 5).

References

- [1] T. Gladman. *The physical metallurgy of microalloyed steels*. London: The Institute of Materials, 2002.
- [2] W. S. Oois and G. Fourlaris. A comparative study of precipitation effects in Ti only and Ti-V Ultra Low Carbon (ULC) strip steels. *Mater. Charact.*, 56:214–226, 2006.
- [3] M. Perez, E. Courtois, D. Acevedo, T. Epicier, and P. Maugis. Precipitation of niobium carbonitrides in ferrite: chemical composition measurements and thermodynamical modelling. *Phil. Mag. Lett.*, 87:645–656, 2007.
- [4] F. Perrard, A. Deschamps, and P. Maugis. Modelling the precipitation of NbC on dislocations in α -Fe. *Acta Mat.*, 55:1255–1266, 2007.
- [5] D. Gendt, P. Maugis, G. Martin, M. Nastar, and F. Soisson. Monte carlo simulation of NbC precipitation kinetics in α -Fe. *Defect and Diffusion Forum*, 194-199:1779–1786, 2001.
- [6] O. H. Bratland, O. Grong, H. R. Shercliff, O. R. Myhr, and S. Tjøtta. Modeling of precipitation reactions in industrial processing. *Acta Mater.*, 45(1):1–22, 1997.
- [7] D. Acevedo-Reyes, M. Perez, S. Pecoraro, A. Vincent, T. Epicier, and P. Dierickx. Vanadium carbide dissolution during austenitisation of a model microalloyed ferrite steel. *Mat. Sc. Forum*, 500-501:695–702, 2005.
- [8] D. Acevedo. *Evolution de l'état de précipitation au cours de l'austénitisation d'aciers microalliés au vanadium et au niobium*. PhD thesis, INSA Lyon, 2007.
- [9] E. Courtois, T. Epicier, and C. Scott. EELS study of niobium carbonitride nano-precipitates in ferrite. *Microns*, 37:492–502, 2006.
- [10] R. G. Baker and J. Nutting. *Precipitation processes in steels*, chapter The tempering of a Cr-Mo-V-W and a Mo-V steel, pages 1–22. Iron and steel institute, 1959.
- [11] J. Billingham, P. S. Bell, and M. H. Lewis. A superlattice with monoclinic symmetry based on the compound V_6C_5 . *Phil. Mag.*, 25:661–671, 1972.
- [12] J. D. Venables, D. Kahn, and R. G. Lye. Structure of the ordered compound V_6C_5 . *Phil. Mag.*, 18:177–192, 1968.
- [13] T. Epicier and Y. Kumashiro. A first HREM observation of the ordered carbon sublattice in a transition metal carbide (VC_{1-x}). *Phil. Mag. Lett.*, 55:171–179, 1987.
- [14] T. Epicier. Application of transmission electron microscopy to the study of transition metal carbides. In R. Freer, editor, *The Physics and Chemistry of Carbides, Nitrides and Borides*, pages 297–327. Kluwer, London, 1990.
- [15] J. D. Venables and R. G. Lye. Radiation damage of ordered V_6C_5 by electron microscope beam bombardment. *Phil. Mag.*, 19:565–582, 1969.
- [16] T. Epicier. HREM visualization of light atoms: an application to the study of carbon defects in ordered transition metal carbides. In *MRS Symp. Proceed.*, pages 255–266, 1990.
- [17] T. Epicier and M. A. O'Keeffe. HRTEM and TEM simulations on a personal computer with simply-S. In UCD, editor, *Proc. XIth Europ. Congress on Electron Microscopy*, Dublin, 1996.
- [18] G. L. Dunlop and D. A. Porter. Secondary precipitation of ordered V_6C_5 and $(V,Ti)_6C_5$ particles in ferrite. *Scand. J. Metall.*, 6:19–20, 1977.
- [19] R. Kesri and S. Hamar-Thibault. Structures ordonnées longue distance dans les carbures MC dans les fontes. *Acta Metall.*, 36:149–166, 1988.
- [20] R. Kesri and M. Durand-Charre. Metallurgical structure and phase diagram of Fe-C-V system: comparison with other systems forming MC carbides. *Mat. Sci. Tech.*, 4:692–699, 1988.
- [21] W. Rong and G. L. Dunlop. The crystallography of secondary carbide precipitation in high speed steel. *Acta Metall.*, 32:1591–1599, 1984.
- [22] J. G. Speer, J. R. Michael, and S. S. Hansen. Carbonitride precipitation in niobium/vanadium microalloyed steels. *Metall. Trans. A*, 18A:211–222, 1987.
- [23] D. Ramakrishna and S. P. Gupta. Coarsening kinetics of vanadium carbide in a high strength, low alloy steel. *Mat. Sc. Eng.*, 92:179–191, 1992.
- [24] G. Fourlaris, A. J. Baker, and G. D. Papadimitriou. A microscopic investigation of the precipitation phenomena observed during the pearlite reaction in vanadium alloyed carbon steels. *Acta Metal. Mater.*, 43:3733–3742, 1995.
- [25] Y. Herrera, I. C. Grigorescu, J. Ramirez, C. Di-Rauso, and M. H. Staia. Microstructural characterization of vanadium carbide laser clad coatings. *Surf. Coat. Tech.*, 198-109:308–311, 1998.
- [26] H. Guanghi and C. Niansun. Effect of Nb in Nb-V microalloyed medium carbon steels. In G. Tither and Z. Shouhua, editors, *HSLA Steels: Processing, Properties and Applications*, pages 411–417. The Minerals, Metals & Materials Society, 1992.
- [27] M. Prikyl, A. Kroupa, G. C. Weatherly, and S. V. Subramanian. Precipitation behavior in a medium carbon, Ti-V-N microalloyed steel. *Metall. Trans. A*, 27A:1149–1165, 1996.
- [28] S. Yamasaki and H. K. D. H. Bhadeshia. Modelling and characterisation of V_4C_3 precipitation and cementite dissolution during tempering of Fe-C-V martensitic steel. *Mat. Sc. Tech.*, 19:1335–1343, 2003.

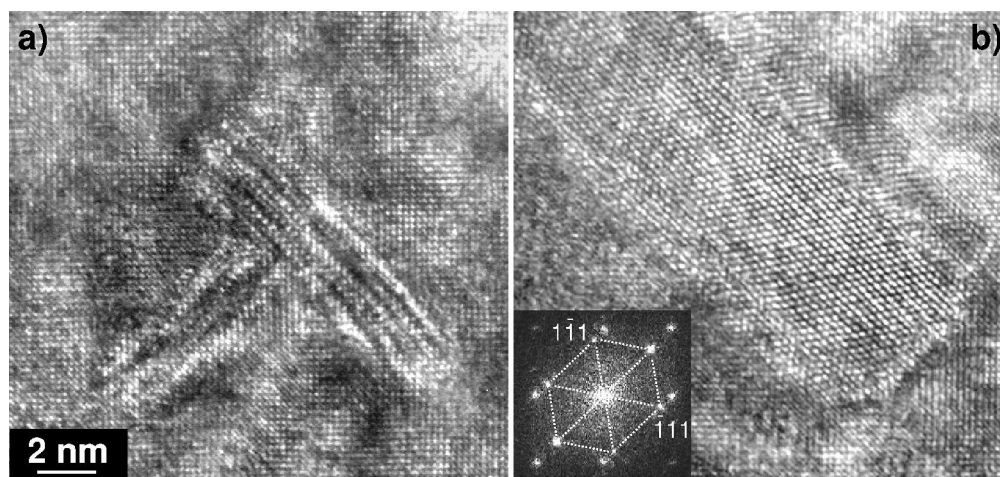
- 1 [29] S. Maropoulos, N. Ridley, and S. Karagiannis. Structural variations in heat treated low alloy steel forgings. *Mat. Sc. Eng.*, A380:79–
2 82, 2004.
- 3 [30] Y. Yazawa, T. Furuhashi, and T. Maki. Effect of matrix recrystallization on morphology, crystallography and coarsening behavior of
4 vanadium carbide in austenite. *Acta Mater.*, 52:3727–3736, 2004.
- 5 [31] S. Shanmugam, M. Tanniru, R. D. K. Misra, D. Panda, and S. Jansto. Microalloyed V-Nb-Ti and V steels part 2 - Precipitation
6 behaviour during processing of structural beams. *Mat. Sc. Tech.*, 21:165–176, 2005.
- 7 [32] E. Smith and J. Nutting. The tempering of low-alloy creep-resistant steels containing chromium, molybdenum, and vanadium. *J.*
8 *Iron Steel Inst.*, 192:314–329, 1957.
- 9 [33] A. K. Seal and R. W. K. Honeycombe. The effect of tantalum and niobium on the tempering of certain vanadium and molybdenum
10 steels. *J. Iron Steels Inst.*, 188:343–350, 1958.
- 11 [34] K. Yvon and E. Parté. On the crystal structure of the close packed transition metal carbides. I. The crystal structure of the ζ -V,
12 Nb and Ta carbides,. *Acta Cryst.*, B26:149–153, 1970.
- 13 [35] T. Fujihana, Y. Okabe, and M. Iwaki. Crystal structure of carbon-implanted titanium, vanadium and chromium. *Nucl. Instr. and*
14 *Meth. in Phys. Res. B*, 127-128:660–663, 1997.
- 15 [36] J. A. Wilson and A. J. Craven. Improving the analysis of small precipitates in HSLA steels using a plasma cleaner and ELNES.
16 *Ultramicroscopy*, 94:197–207, 2003.
- 17 [37] E. K. Storms and R. J. McNeal. The vanadium-vanadium carbide system. *J. Phys. Chem.*, 66:1401–1408, 1962.
- 18 [38] M. H. Lewis, J. Bellingham, and J. Bell. *Electron Microscopy and Structure of Materials*, chapter Non-stoichiometry in ceramic
19 compounds, pages 1084–1115. University of California Press: Berkeley, 1972.
- 20 [39] J. L. Martin, A. Rocher, B. Jouffrey, and P. Costa. electron diffraction of the (Ta C) phase. *Phil. Mag.*, 24:1355–1364, 1971.
- 21 [40] D. J. Rowcliffe and G. Thomas. structure of non-stoichiometric TaC. *Mat. Sci. Eng.*, 18:231–238, 1975.
- 22
23
24
25
26
27
28
29
30
31
32
33
34
35
36
37
38
39
40
41
42
43
44
45
46
47
48
49
50
51
52
53
54
55
56
57
58
59
60

1
2
3
4
5
6
7
8
9
10
11
12
13
14
15
16
17
18
19
20
21
22
23
24
25
26
27
28
29
30
31
32
33
34
35
36
37
38
39
40
41
42
43
44
45
46
47
48
49
50
51
52
53
54
55
56
57
58
59
60

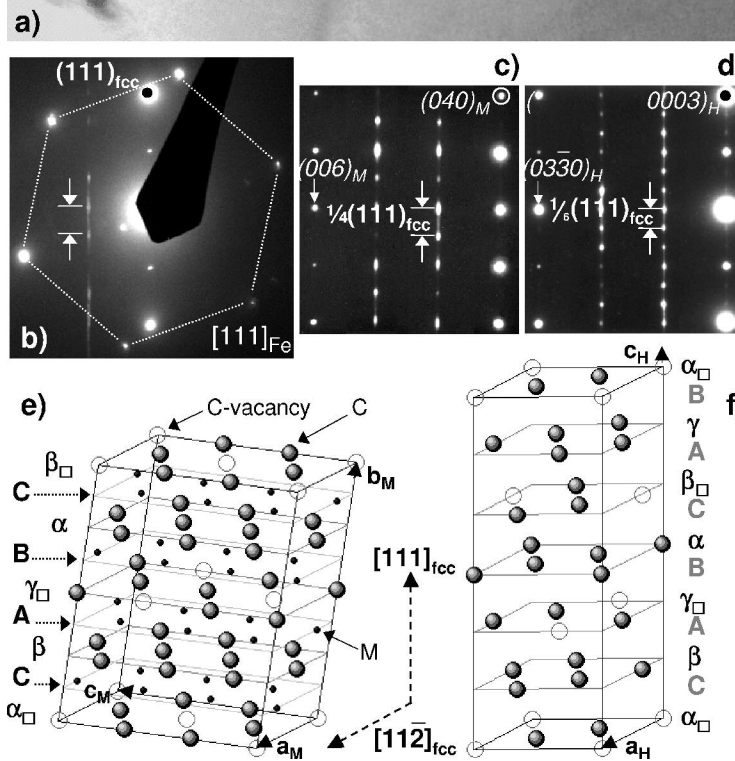
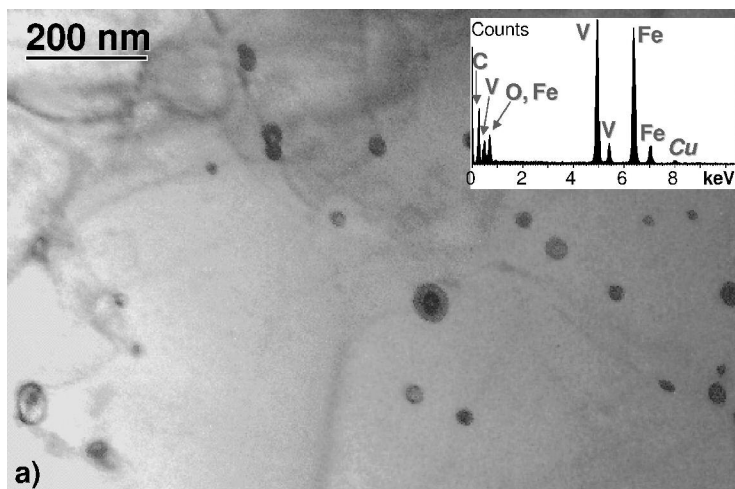


178x157mm (600 x 600 DPI)

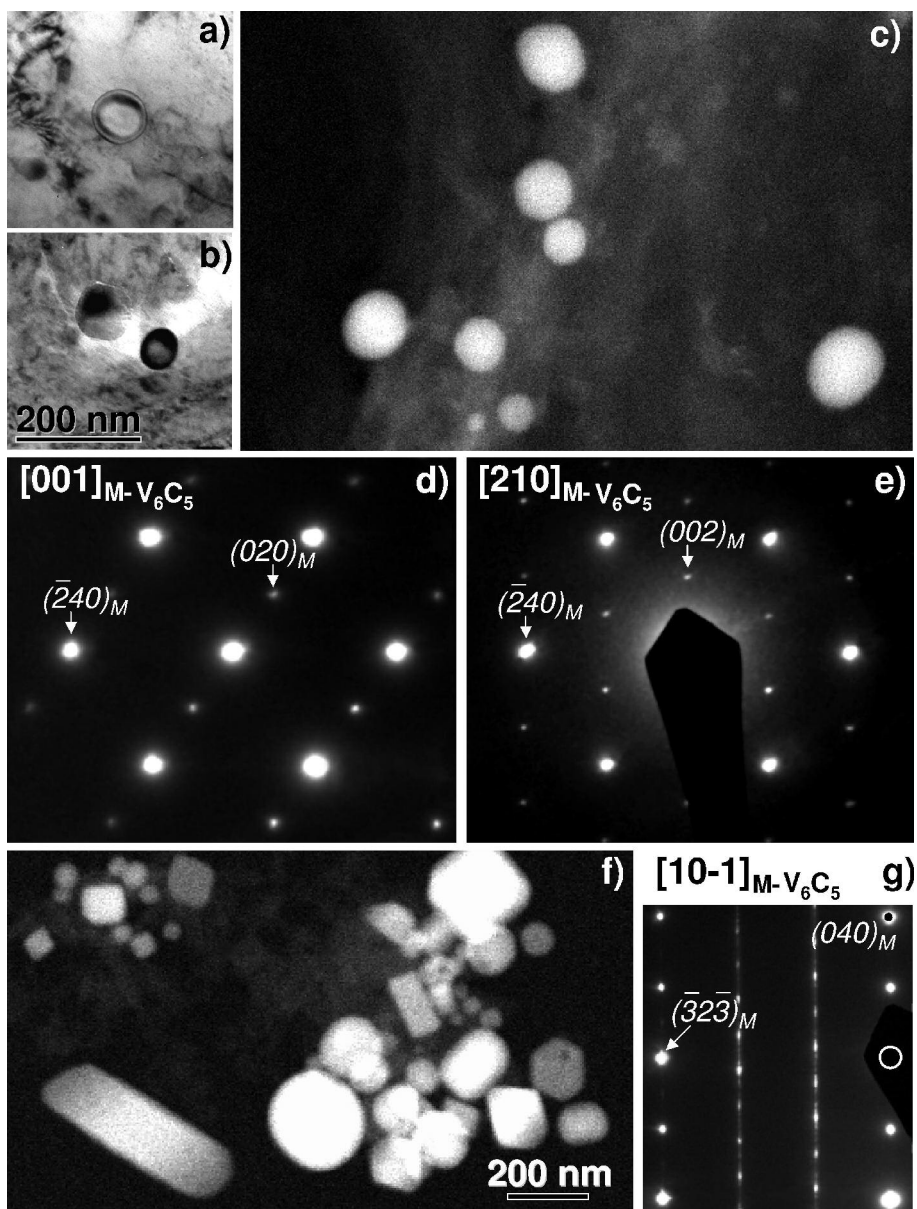
View Only



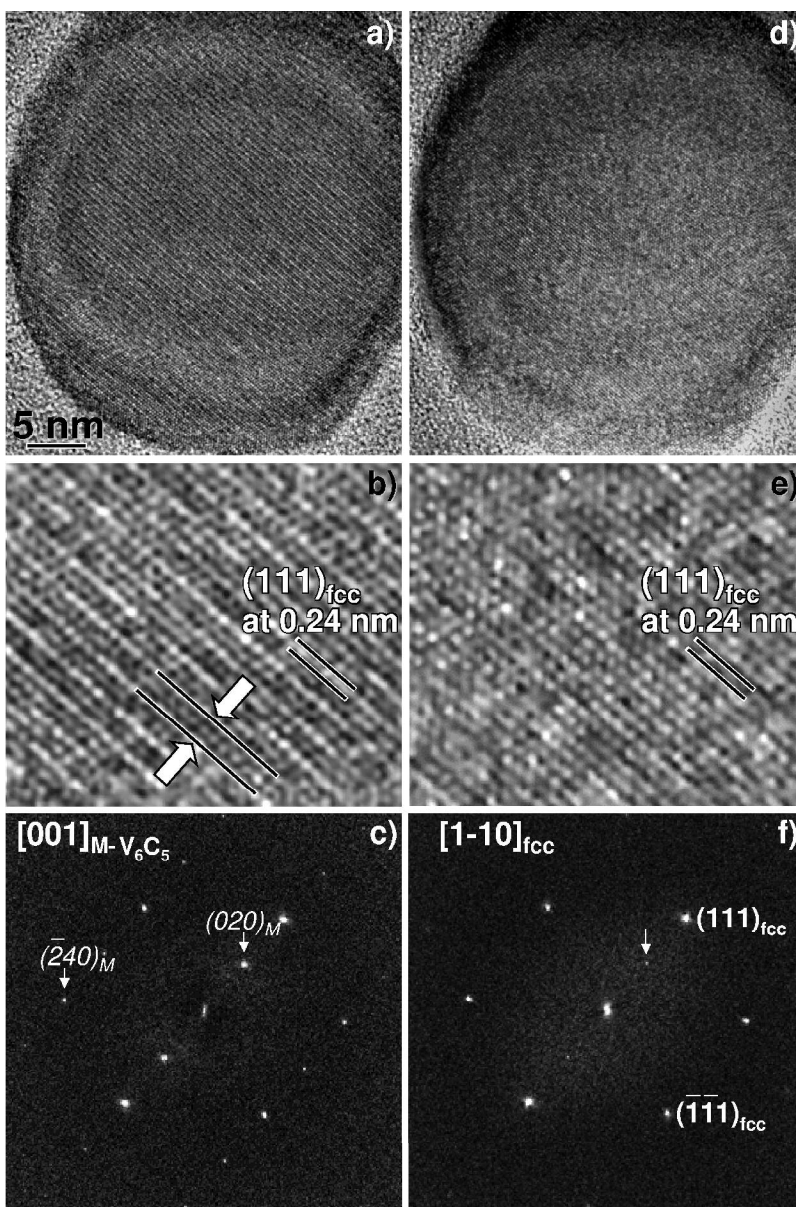
183x86mm (600 x 600 DPI)



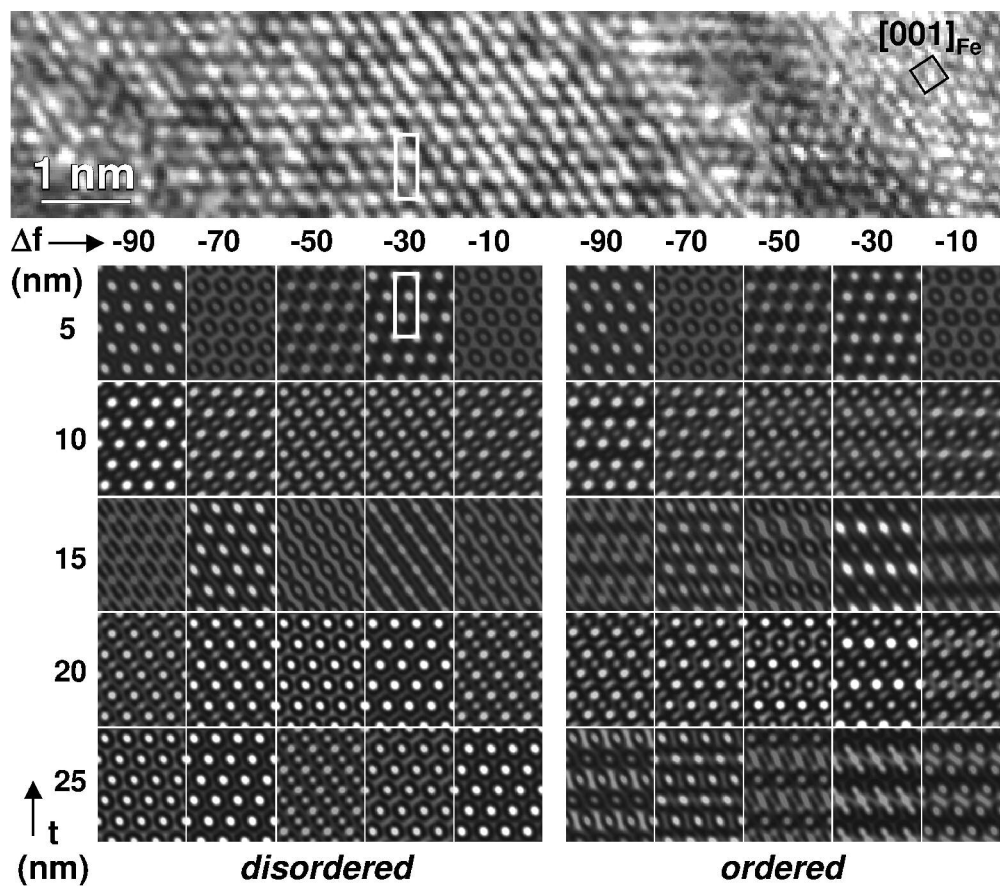
141x230mm (600 x 600 DPI)



141x187mm (600 x 600 DPI)



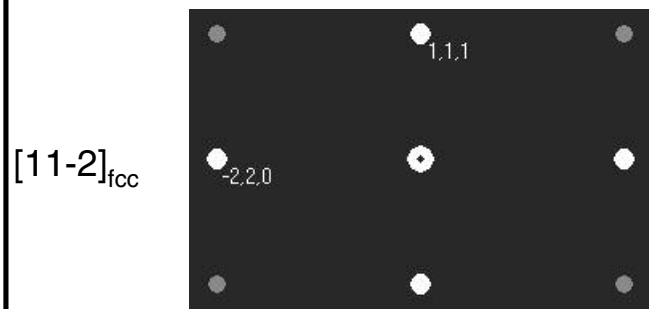
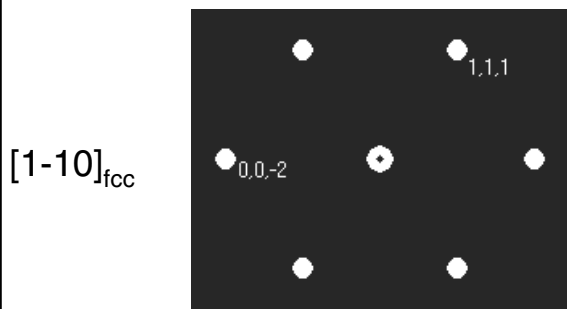
141x212mm (600 x 600 DPI)



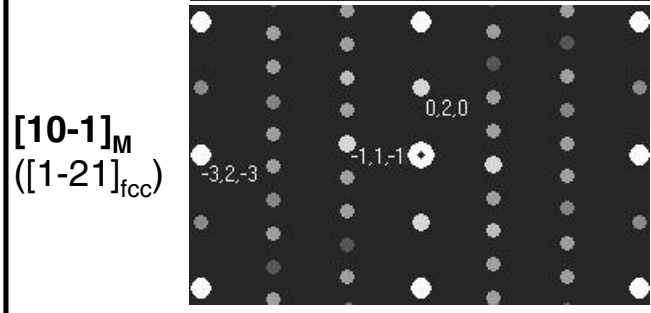
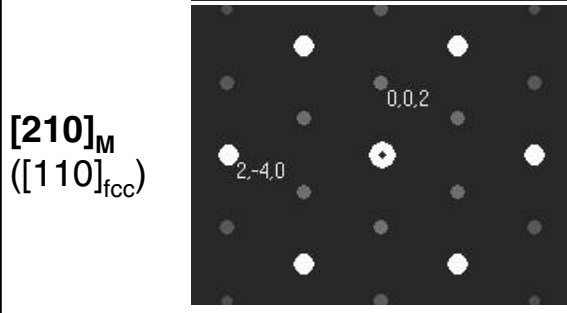
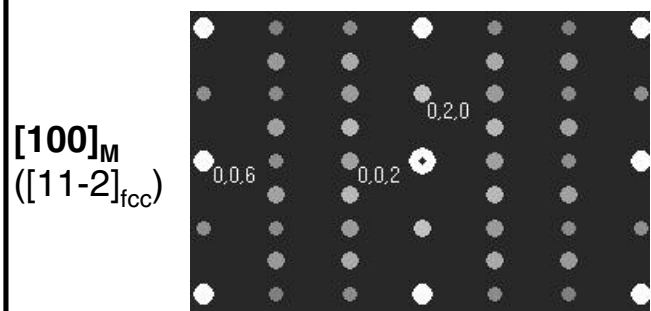
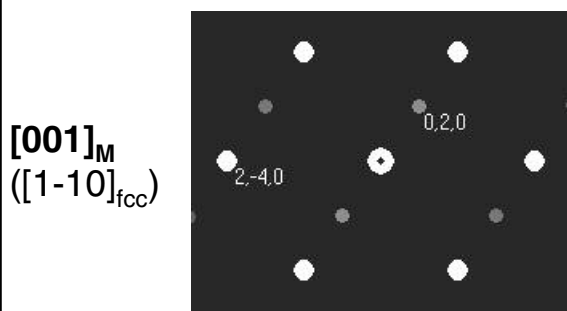
190x166mm (600 x 600 DPI)

Only

1
2
3
4
5 ***fcc VC***
6
7
8
9
10

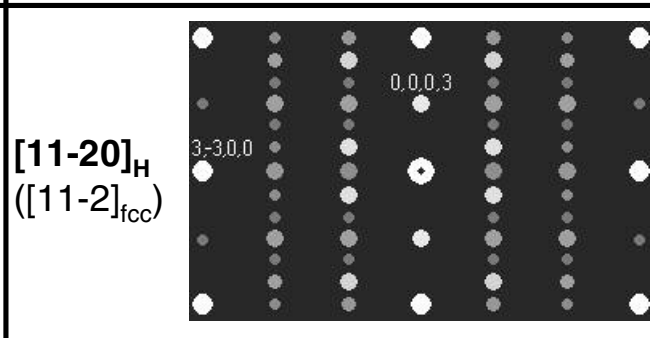
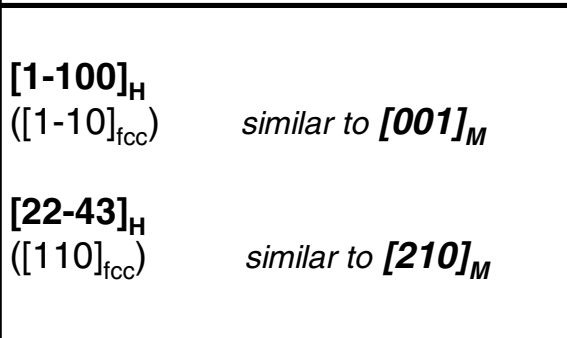


11
12
13
14
15
16
17
18
19
20
21 ***monoclinic***
22 ***V₆C₅***
23
24
25
26
27
28
29
30



31
32
33
34
35
36
37
38
39
40
41

hexagonal
V₆C₅



42
43
44
45
46
47
48
49
50
51
52

trigonal
V₄C₃

